Systematic Analysis of Core Photoemission Spectra for Actinide Di-Oxides and Rare-Earth Sesqui-Oxides

Akio KOTANI and Takao YAMAZAKI*,*)

Institute for Solid State Physics, University of Tokyo, Tokyo 106
**Department of Physics, Tohoku University, Sendai 980*

(Received September 4, 1991)

We carry out systematic analysis of $4f$ core photoemission spectra for actinide di-oxides AnO_2 (An=Th~Bk), using the impurity Anderson model including the exchange interaction J between $5f$ electrons. The effect of J is important in explaining the observed photoemission spectra especially for PuO_2, AmO_2 and CmO_2. It is shown that PuO_2 and BkO_2 are strongly mixed valence compounds, and that a crossover between Mott-Hubbard-type and charge-transfer-type insulators occurs around NpO_2. A previous analysis of $3d$ core photoemission spectra for rare-earth sesqui-oxides R_2O_3 (R=La~Yb) is briefly reviewed, and the results for AnO_2 and R_2O_3 are compared.

§ 1. Introduction

Core-level spectroscopy provides us with important information on the electronic structure in solids.[1] The impurity Anderson model has been used successfully in the analysis of core-level X-ray photoemission spectra (XPS) in various rare-earth compounds[2] and transition-metal compounds.[3]

For a series of rare-earth sesqui-oxides R_2O_3 (R=La~Yb), Ikeda et al.[4),5] recently analyzed the $3d$ core X-ray photoemission spectra ($3d$-XPS) with the impurity Anderson model. They showed that the charge transfer energy Δ and the hybridization strength V between the rare-earth $4f$ state and the O$2p$ state changes systematically with the atomic number of the rare-earth element, where Δ is defined by the energy which is necessary to transfer an O$2p$ valence electron to the rare-earth $4f$ state. According to them, Δ decreases from La to Eu, jumps to a larger value at Gd, and decreases again from Gd to Yb, while V decreases almost monotonically.

Compared with rare-earth compounds, much less study has been made for actinide compounds. The purpose of the present paper is to present a systematic analysis[6] of actinide $4f$ core XPS in actinide di-oxide series (AnO_2) using the impurity Anderson model, and to compare the result with that of R_2O_3. Figure 1 shows the experimental data of actinide $4f$-XPS in ThO_2~BkO_2.[7)~9] For ThO_2~PuO_2, the $4f$-XPS exhibits, in its $4f_{7/2}$ and $4f_{5/2}$ components, a satellite peak about 7 eV above the main peak. The intensity of the satellite increases from Th to Pu, but it decreases rapidly for Am and almost vanishes for Cm. The $4f$-XPS of BkO_2 has two satellite

*) Present address: Computational Science Research Laboratory, Fujitsu Ltd., Shinkamata, Ota-ku, Tokyo 144.

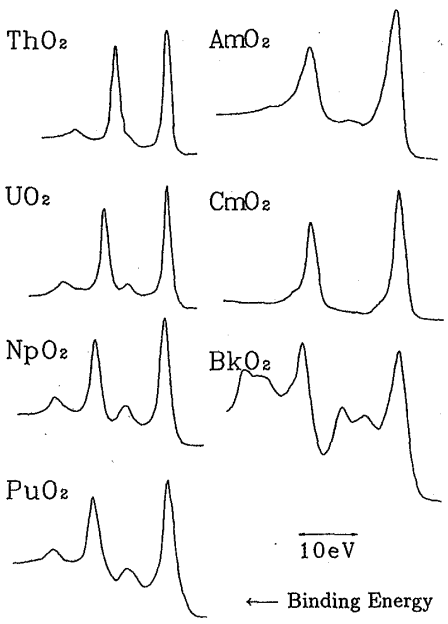

Fig. 1. Experimental results of $4f$-XPS for AnO_2 (An=Th, U~Bk). The result for ThO_2 is taken from Ref. 7), that for UO_2 is from Ref. 8) and others are from Ref. 9).

peaks about 6.0 eV and 9.7 eV above the main peak. The width of the main peak increases gradually from Th to Am, with the maximum value for Am, and it decreases for Cm and Bk.

An analysis of the $4f$-XPS for ThO_2, UO_2 and NpO_2 was made by Gunnarsson and Sarma[7] with the impurity Anderson model. The increase of the satellite intensity from Th to Np is understood, as will be discussed later, from the fact that the charge transfer energy Δ decreases with increasing atomic number. However, when we apply a similar analysis to PuO_2, AmO_2 and CmO_2, we obtain too large a satellite intensity, unless we assume that Δ increases with the atomic number. In the present paper, we extend the usual impurity Anderson model by introducing the exchange interaction J between $5f$ electrons. Then the analysis for $ThO_2 \sim BkO_2$ can be made with reasonable behavior of Δ, which decreases from Th to Cm and jumps at Bk, in a consistent manner with the case of R_2O_3 (note that "Bk^{4+}" corresponds to "Gd^{3+}" with half-filled f electrons). It will also be shown that a crossover between the Mott-Hubbard-type and the charge-transfer-type insulators occurs around NpO_2, and that PuO_2 and BkO_2 are strongly mixed valence compounds.

In § 2, the model and the method of calculating $4f$-XPS for AnO_2 are described. The calculated results are shown in § 3, where the effect of J and the systematic variation of the other parameters are also discussed. In § 4, the result of the analysis of rare-earth $3d$-XPS for R_2O_3 is briefly reviewed, and compared with the actinide $4f$-XPS for AnO_2. Section 5 is devoted to concluding remarks.

§ 2. Formulation

2.1. *Model*

We consider a system which consists of an O$2p$ valence band and $5f$ electrons on a single actinide atom. The Hamiltonian is given by

$$H_0=\sum_{k,m,\sigma}\varepsilon_v(k)n_{km\sigma}+\varepsilon_f\sum_{m,\sigma}n_{fm\sigma}+\frac{1}{2}(U-J)\sum_{m,m',\sigma(m\neq m')}n_{fm\sigma}n_{fm'\sigma}$$
$$+U\sum_{m,m'}n_{fm\uparrow}n_{fm'\downarrow}+\frac{V}{\sqrt{N}}\sum_{k,m,\sigma}(a^{\dagger}_{km\sigma}a_{fm\sigma}+a^{\dagger}_{fm\sigma}a_{km\sigma}), \qquad (2\cdot1)$$

where $\varepsilon_v(k)$ is the energy of the O$2p$ valence band with the index $k(=1\sim N)$ specifying the energy level, ε_f is the $5f$ level, U and J are, respectively, the Coulomb and

exchange interactions between $5f$ electrons, and V is the hybridization between $5f$ and valence electrons. The operator $a_{im\sigma}(i=k, f)$ represents the annihilation of an electron in the state (i, m, σ), where m and σ are the indices specifying the orbital and spin degeneracies of the f state, respectively, and $n_{im\sigma}$ is the number operator: $n_{im\sigma}=a^{\dagger}_{im\sigma}a_{im\sigma}$.

In the final state of $4f$-XPS, a core hole is created in the $4f$ level, and then the $5f$ level is pulled down by the core hole potential. Thus the Hamiltonian describing the final state is written as

$$H=H_0-U_{fc}\sum_{m,\sigma}n_{fm\sigma}\,, \tag{2·2}$$

whehe $-U_{fc}$ is the core hole potential acting on the $5f$ electron.

The Hamiltonians (2·1) and (2·2) are diagonalized numerically for a finite system where $\varepsilon_v(k)$ is expressed as

$$\varepsilon_v(k)=\varepsilon_v-\frac{W}{2}+\frac{W}{N}\left(k-\frac{1}{2}\right),\quad (k=1\sim N) \tag{2·3}$$

and with the basis states given in § 2.2. In Eq. (2·3), ε_v and W represent the center and the width of the valence band, respectively. The value of N is taken to be sufficiently large so that the calculated spectrum converges well. The photoemission spectrum is represented by

$$F(E_B)=\sum_f|\langle f|g\rangle|^2\frac{\Gamma/\pi}{(E_B-E_f+E_g)^2+\Gamma^2}\,, \tag{2·4}$$

where $|g\rangle$ is the ground state of H_0 with energy E_g, $|f\rangle$ are eigenstates of H with energies E_f, E_B is the binding energy, and Γ represents the spectral broadening corresponding to the lifetime of the core hole. We also take into account a Gaussian broadening corresponding to the experimental resolution.

2.2. *Basis states*

In the limit of vanishing V, we define $|f^n\rangle$ by the state where the valence band is filled and n $5f$ electrons with $\uparrow$ spin are occupied. Then $|f^n\rangle$ is written as

$$|f^n\rangle=\prod_{m=1}^{n}a^{\dagger}_{fm\uparrow}|f^0\rangle\,, \tag{2·5}$$

where

$$|f^0\rangle=\prod_{k=1}^{N}\prod_{m=1}^{N_f}\prod_{\sigma=\uparrow\downarrow}a^{\dagger}_{km\sigma}|\mathrm{vac}\rangle \tag{2·6}$$

with the vacuum state $|\mathrm{vac}\rangle$ and with $N_f=7$. Here, we confine ourselves to the case $n\leq 7$, and take $n=0, 2, 3\cdots 7$ for Th, U, Np$\cdots$Bk, respectively. When the hybridization V is switched on, $|f^n\rangle$ is coupled with the states $|f^{n+1}\uparrow\underline{L}(k)\rangle$ and $|f^{n+1}\downarrow\underline{L}(k)\rangle$, where $|f^{n+1}\uparrow\underline{L}(k)\rangle$, for instance, denotes the state obtained from $|f^n\rangle$ by transferring a valence electron with k and $\uparrow$ spin to the $5f$ state (for Bk, $|f^{n+1}\uparrow\underline{L}(k)\rangle$ should be excluded because of the Pauli principle). The state $|f^{n+1}\uparrow\underline{L}(k)\rangle$ and $|f^{n+1}\downarrow\underline{L}(k)\rangle$ are written as

$$|f^{n+1}\uparrow \underline{L}(k)\rangle=\frac{1}{\sqrt{N_f-n}}\sum_{m=n+1}^{N_f} a^\dagger_{fm\uparrow}a_{km\uparrow}|f^n\rangle\,, \tag{2·7}$$

$$|f^{n+1}\downarrow \underline{L}(k)\rangle=\frac{1}{\sqrt{N_f}}\sum_{m=1}^{N_f} a^\dagger_{fm\downarrow}a_{km\downarrow}|f^n\rangle\,. \tag{2·8}$$

These states are also coupled through V with the states

$$|f^{n+2}\uparrow\uparrow \underline{L}^2(k,l)\rangle=\frac{\delta_2(k,l)}{\sqrt{(N_f-n)(N_f-n-1)}}\sum_{m\neq m'=n+1}^{N_f} a^\dagger_{fm\uparrow}a_{km\uparrow}a^\dagger_{fm'\uparrow}a_{lm'\uparrow}|f^n\rangle\,, \tag{2·9}$$

$$|f^{n+2}\uparrow\downarrow \underline{L}^2(k,l)\rangle=\frac{1}{\sqrt{N_f(N_f-n)}}\sum_{m=n+1}^{N_f}\sum_{m'=1}^{N_f} a^\dagger_{fm\uparrow}a_{km\uparrow}a^\dagger_{fm'\downarrow}a_{lm'\downarrow}|f^n\rangle\,, \tag{2·10}$$

$$|f^{n+2}\downarrow\downarrow \underline{L}^2(k,l)\rangle=\frac{\delta_2(k,l)}{\sqrt{N_f(N_f-1)}}\sum_{m\neq m'=1}^{N_f} a^\dagger_{fm\downarrow}a_{km\downarrow}a^\dagger_{fm'\downarrow}a_{lm'\downarrow}|f^n\rangle\,, \tag{2·11}$$

unless the coupling is forbidden by the Pauli principle. Here $\delta_2(k,l)$ is given by

$$\delta_2(k,l)=\begin{cases}1 & \text{for}\quad k\neq l\,,\\ 1/\sqrt{2} & \text{for}\quad k=l\,.\end{cases} \tag{2·12}$$

The states (2·9)~(2·11) are then coupled with $|f^{n+3}\uparrow\uparrow\uparrow \underline{L}^3(k,l,m)\rangle$, $|f^{n+3}\uparrow\uparrow\downarrow \underline{L}^3(k,l,m)\rangle$, $|f^{n+3}\uparrow\downarrow\downarrow \underline{L}^3(k,l,m)\rangle$ and $|f^{n+3}\downarrow\downarrow\downarrow \underline{L}^3(k,l,m)\rangle$, whose expressions are not given here explicitly.

In order to obtain the ground state $|g\rangle$ and final states $|f\rangle$, we use the basis states from $|f^n\rangle$ to $|f^{n+3}\downarrow\downarrow\downarrow \underline{L}^3(k,l,m)\rangle$. Hamiltonian matrix elements for these basis states are given in the Appendix.

§ 3. Calculated results

The calculated XPS spectra are shown in Figs. 2(a)~(g) for ThO_2~BkO_2, respectively. The solid curve is obtained by convoluting the original line spectra with a Lorentzian function of width 1.0 eV (FWHM) and a Gaussian function of width 1.1 eV (FWHM), and by adding a background contribution $B(E_B)$ (the dashed curve). The spectrum $B(E_B)$ is calculated by assuming the relation

$$B(E_B)=C\int_{-\infty}^{E_B}F(E'_B)dE'_B \tag{3·1}$$

with a constant C as an adjustable parameter. In Fig. 2 the origin of E_B is taken arbitrarily. The main parameter values used in our calculations are listed in Table I. With these parameters, the $5f$ electron number n_f averaged in the ground state is also estimated and shown in Table I.

In this analysis, we assume that the value U in the initial state (denoted by $(U(i))$ is a little smaller than that in the final state $(U(f))$, and we take account of the fact that U and U_{fc} increases and V decreases with increasing atomic number. The value of J is taken from Van der Marel's paper[10] as follows:

$$J=0.33+0.07(Z-89)(\text{eV})\,, \tag{3·2}$$

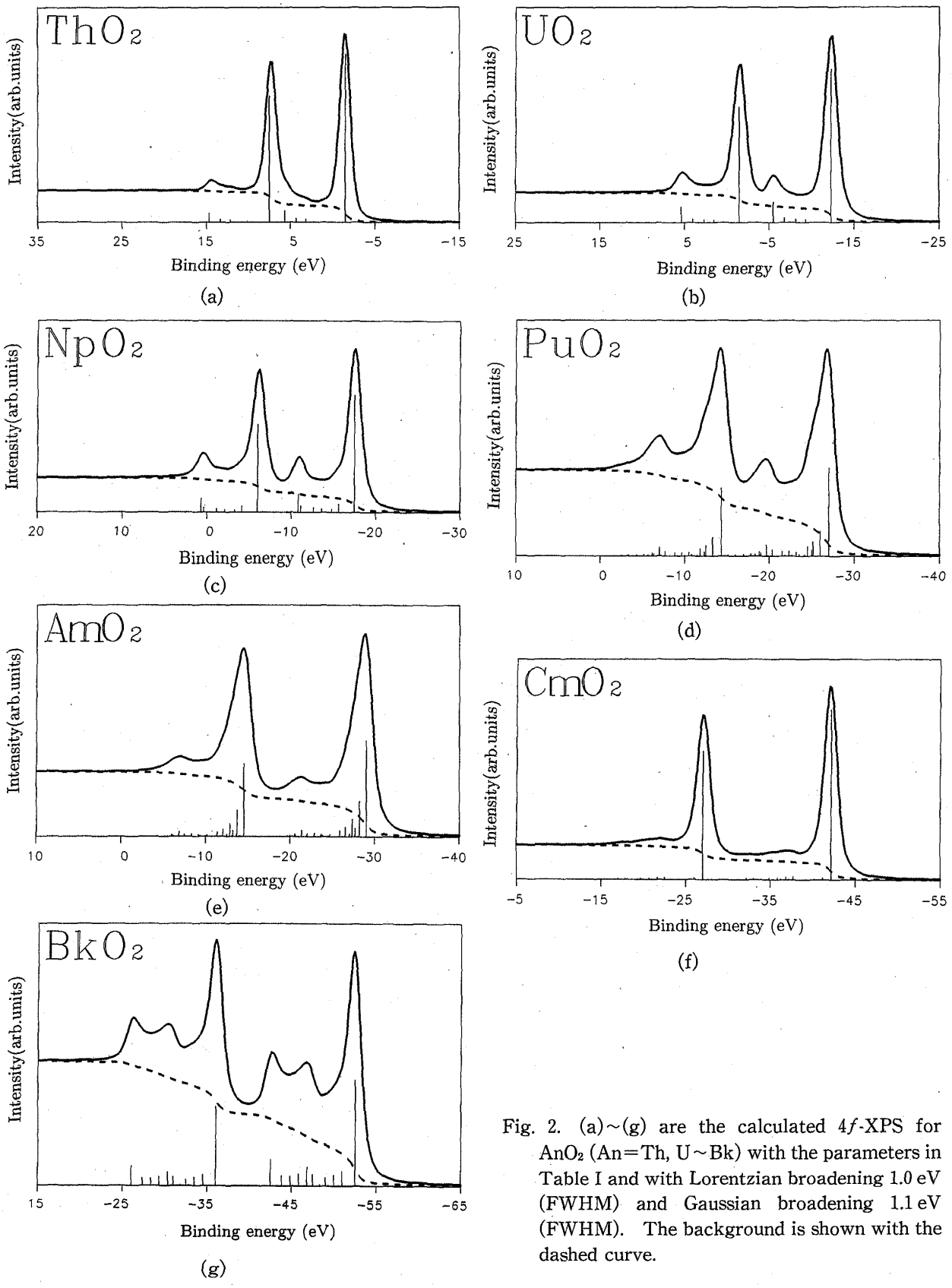

Fig. 2. (a)~(g) are the calculated $4f$-XPS for AnO_2 (An=Th, U~Bk) with the parameters in Table I and with Lorentzian broadening 1.0 eV (FWHM) and Gaussian broadening 1.1 eV (FWHM). The background is shown with the dashed curve.

Table I. The parameter values for AnO_2 (An=Th~Bk) estimated from the present analysis (in units of eV except for n and n_f).

	n	Δ	Δ_f	V	$U(i)$	$U(f)$	U_{fc}	J	W	n_f
Th	0	9.00	4.00	1.05	4.00	4.25	5.00	0.40	3.00	0.17
U	2	6.42	1.42	1.15	4.50	4.75	5.50	0.54	3.00	2.26
Np	3	3.92	−0.88	1.10	5.00	5.35	5.85	0.61	3.00	3.36
Pu	4	0.78	−4.47	0.95	5.50	5.75	6.25	0.68	3.50	4.65
Am	5	−0.25	−5.35	0.90	6.00	6.40	7.10	0.75	3.50	5.83
Cm	6	−0.72	−6.67	0.90	6.70	7.00	7.75	0.82	4.00	6.97
Bk	7	2.07	−4.70	0.875	7.28	7.49	8.24	0.89	4.00	7.49

where Z is the atomic number.

In order to see the effect of J, we show in Fig. 3 the coupling scheme of the basis states through the hybridization. If we disregard the effect of J, $|f^n\rangle$ is coupled with $|f^{n+1}\underline{L}(k)\rangle$ ($\underline{L}(k)$ will be simply written as $\underline{L}$ hereafter) with the matrix element $\sqrt{14-n}(V/\sqrt{N})$, in other words, with the effective hybridization strength $V_{\rm eff}=\sqrt{14-n}\,V$. When we take into account J, the state $|f^{n+1}\underline{L}\rangle$ splits into $|f^{n+1}\uparrow\underline{L}\rangle$ and $|f^{n+1}\downarrow\underline{L}\rangle$ whose energy separation is nJ (exchange splitting). If n is not very small, this splitting is important [for AmO_2 ($n=5$), for instance, $nJ\simeq 3.7$ eV]. Further, the value of $V_{\rm eff}$ between $|f^n\rangle$ and $|f^{n+1}\uparrow\underline{L}\rangle$ is different from that between $|f^n\rangle$ and $|f^{n+1}\downarrow\underline{L}\rangle$; the former is $\sqrt{7-n}\,V$, while the latter is $\sqrt{7}\,V$ (see the Appendix). Thus the effect of J is to cause the exchange splitting and the corresponding modification of $V_{\rm eff}$. The values of $V_{\rm eff}$ with respect to the basis states $|f^{n+2}\uparrow\uparrow\underline{L}^2\rangle\sim|f^{n+3}\downarrow\downarrow\downarrow\underline{L}^3\rangle$ are also shown in Fig. 3.*)

The value of Δ in Table I is given by the energy difference between $|f^{n+1}\sigma\underline{L}\rangle$ and $|f^n\rangle$ (before switching on V). Here, the energy of $\underline{L}$ is taken to be the center of the valence band, and $\sigma=\uparrow$ for Th~Cm but $\sigma=\downarrow$ for Bk because the state $|f^n\rangle$ of Bk is half-filled. It is found that Δ decreases monotonically from Th to Cm, but it increases at Bk because of the change of the exchange energy contribution by $6J$ between Cm and Bk. Note that the explicit form of Δ is written as follows:

$$\Delta=\varepsilon_f-\varepsilon_v+nU(i)-n_1J \qquad (3\cdot3)$$

with

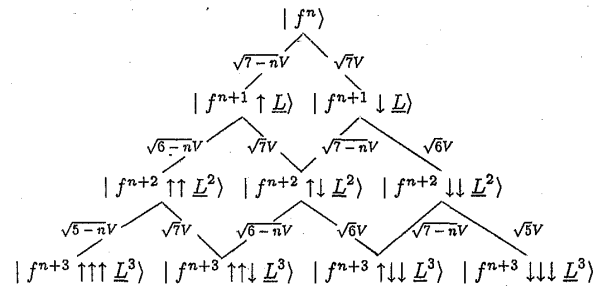

Fig. 3. The basis states used in our calculations and the strengths of effective hybridization acting between these states. The definition of these basis states is given in the text. The two states linked with a line hybridize with the strength shown beside the line.

*) In more detail, the value $V_{\rm eff}$ between $|f^{n+1}\sigma\underline{L}(k)\rangle$ and $|f^{n+2}\sigma\sigma'\underline{L}(l,m)\rangle$, for instance, depends on k, l and m. We show in Fig. 3 the most dominant contribution from $k=l\neq m$ (or $k=m\neq l$) for large N (see the Appendix).

$$n_1=\begin{cases} n & \text{for } n\leq 6, \\ n-7 & \text{for } n\geq 7. \end{cases} \tag{3·4}$$

The calculated XPS spectra are in good agreement with the experimental data. For $ThO_2 \sim NpO_2$, the effect of J is not very important because of the small $5f$ electron number n. In the case of ThO_2, the value of Δ is considerably larger than V_{eff}, so that the ground state is mainly in the $|f^0\rangle$ state. On the other hand, the energy difference between the states $|f^1\underline{L}\rangle$ and $|f^0\rangle$ decreases in the final state due to the core hole potential $-U_{fc}$, and becomes comparable with V_{eff}. We denote this energy difference as Δ_f (the charge transfer energy in the final state). Therefore, the main peak of $4f$-XPS corresponds to the bonding state (mainly with $|f^0\rangle$ component) between $|f^0\rangle$ and $|f^1\underline{L}\rangle$ states and the satellite the antibonding state (mainly with $|f^1\underline{L}\rangle$ component). As going from ThO_2 to NpO_2, both of Δ and $|\Delta_f|$ decrease. Especially due to the decrease of $|\Delta_f|$, the final state mixing between $|f^0\rangle$ and $|f^1\underline{L}\rangle$ increases, so that the intensity of the satellite increases. For general n, Δ_f is expressed as

$$\begin{aligned} \Delta_f &= \varepsilon_f - \varepsilon_v + nU(f) - U_{fc} - n_1 J \\ &= \Delta - U_{fc} + n[U(f) - U(i)] \end{aligned} \tag{3·5}$$

with n_1 given by Eq. (3·4), and the value of Δ_f is also listed in Table I. From the value n_f in Table I, it is to be noted that the initial state mixing between $|f^0\rangle$ and $|f^1\underline{L}\rangle$ is also considerably large for UO_2 and NpO_2.

For Pu and Am, Δ is small, and the effect of the hybridization is very important both in the initial and final states. The effect to J is also important. The ground state of PuO_2 consists of $|f^n\rangle$, $|f^{n+1}\uparrow \underline{L}\rangle$ and $|f^{n+1}\downarrow \underline{L}\rangle$ states with the weight of 42%, 37% and 14%, respectively. For AmO_2, these weights change into 25%, 61% and 7%, respectively, because Δ becomes slightly negative. Both for Pu and Am, the final states of the main peak are the mixed states between $|f^{n+1}\uparrow \underline{L}\rangle$ and $|f^{n+2}\uparrow\uparrow \underline{L}^2\rangle$ states, and those of the satellite are the mixed states among $|f^n\rangle$, $|f^{n+1}\downarrow \underline{L}\rangle$ and $|f^{n+2}\uparrow \underline{L}^2\rangle$ states. As going from PuO_2 to AmO_2, the initial weight of the $|f^n\rangle$ state decreases, so that the intensity of the satellite becomes smaller.

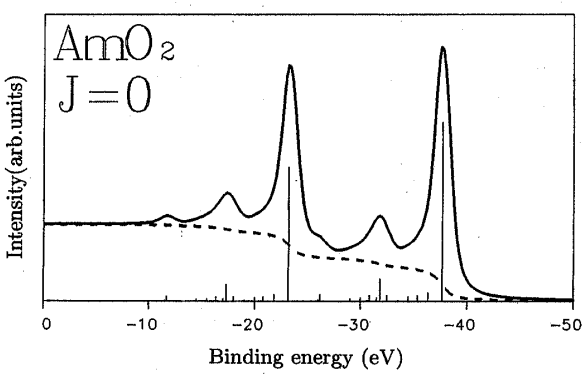

Fig. 4. The calculated $4f$-XPS for AmO_2 with $J=0.0$ eV, where the other parameters are the same as those for AmO_2 in Table I.

To see the role of J, we show in Fig. 4 the calculated XPS spectrum for AmO_2 with vanishing J (Δ and Δ_f are kept unchanged). In this case, the width of the main peak is smaller, and the satellite becomes more remarkable, compared with the case $J\neq 0$ (Fig. 2(e)). Furthermore, a second satellite peak about 12 eV above the main peak occurs. For $J=0$, the main peak and the first satellite correspond to the bonding and antibonding states (bound states) between $|f^6\underline{L}\rangle$ and $|f^7\underline{L}^2\rangle$ final states, which are coupled strongly by the

effective hybridization $V_{\rm eff}=\sqrt{8}V$. The second satellite corresponds mainly to $|f^5\rangle$ final state. When J is switched on, $|f^6\underline{L}\rangle$ splits into $|f^6\uparrow\underline{L}\rangle$ and $|f^6\downarrow\underline{L}\rangle$, and $|f^7\underline{L}^2\rangle$ splits into $|f^7\uparrow\uparrow\underline{L}^2\rangle$, $|f^7\uparrow\downarrow\underline{L}^2\rangle$ and $|f^7\downarrow\downarrow\underline{L}^2\rangle$. Then the main peak consists of $|f^6\uparrow\underline{L}\rangle$ and $|f^7\uparrow\uparrow\underline{L}^2\rangle$ final states, and the satellite $|f^5\rangle$, $|f^6\downarrow\underline{L}\rangle$ and $|f^7\uparrow\downarrow\underline{L}^2\rangle$ final states, as mentioned before. The coupling between $|f^6\uparrow\underline{L}\rangle$ and $|f^7\uparrow\uparrow\underline{L}^2\rangle$ is very small with $V_{\rm eff}=V$, so that the main peak intensity is spread over the valence band width (because of the valence hole $\underline{L}$) instead of forming a strong bound state. The intensity of the satellite is also spread widely because of the exchange splitting. Thus, the effect of J makes the main peak width larger, and the satellite less conspicuous, in a manner consistent with experiments.

The situation in Cm is somewhat anomalous. Since Δ is negative, the ground state configuration is mainly $|f^7\uparrow\underline{L}\rangle$, where the contribution from $|f^6\rangle$, $|f^7\downarrow\underline{L}\rangle$ and $|f^8\uparrow\downarrow\underline{L}^2\rangle$ are much smaller because of the higher energy (note that the $|f^8\uparrow\uparrow\underline{L}\rangle$ state is impossible). The final state of the XPS peak is also the $|f^7\uparrow\underline{L}\rangle$ state, and the other states which hybridize with this state give only weak and widely spread spectra. The situation is simple in Bk, because we only take account of $|f^7\rangle$, $|f^8\downarrow\underline{L}\rangle$, $|f^9\downarrow\downarrow\underline{L}^2\rangle$ and $|f^{10}\downarrow\downarrow\downarrow\underline{L}^3\rangle$ states and no lift of the spin degeneracy occurs. The value of Δ is comparable with the effective hybridization $\sqrt{7}V$, so that the ground state is a strongly mixed state between $|f^7\rangle$ and $|f^8\downarrow\underline{L}\rangle$ states. The three XPS peaks originate from $|f^7\rangle$, $|f^8\downarrow\underline{L}\rangle$ and $|f^9\downarrow\downarrow\underline{L}^2\rangle$ final states, where the latter two states are strongly mixed through the hybridization. In this respect, the origin of the three XPS peaks of BkO_2 is similar to that in $3d$-XPS of CeO_2[2] and PrO_2.[11]

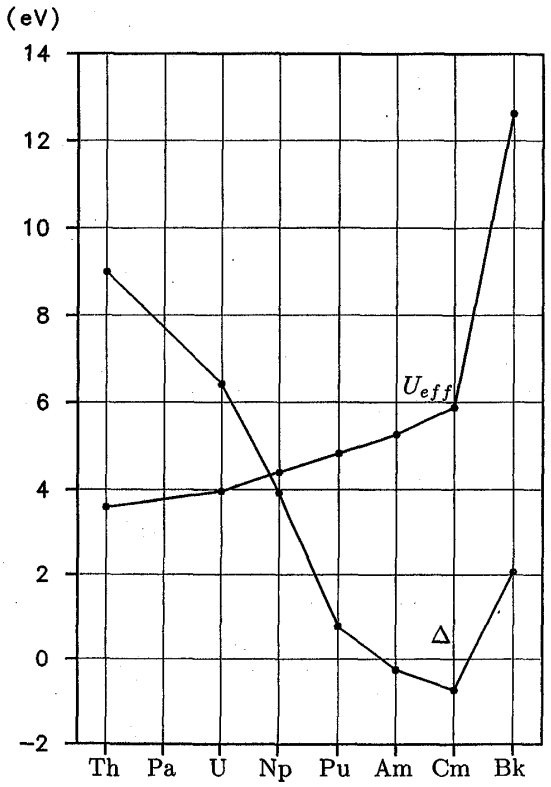

Fig. 5. The effective correlation energy $U_{\rm eff}$ and the charge transfer energy Δ estimated for a series of AnO_2 (An=Th~Bk).

From our analysis, it is found that PuO_2 and BkO_2 are materials of strong mixed-valence with $n_f\sim4.6$ and $n_f\sim7.5$, respectively. AmO_2 and CmO_2 have n_f values much larger than those of the tetravalent ion; especially for CmO_2 the value of n_f is almost that of the trivalent ion. This may suggest that CmO_2 has an almost unstable crystalline structure.[12]

We can estimate from our results the magnitude of the correlation gap, which is the insulating energy gap corresponding to the charge fluctuation

$$f_i^n f_j^n \leftrightarrow f_i^{n-1} f_j^{n+1},$$

where i and j label actinide ion sites. The correlation gap is given by the effective Coulomb energy

$$U_{\rm eff}=\begin{cases} U-J & \text{for } n\leq 6 \\ U+6J & \text{for } n=7. \end{cases} \quad (3\cdot6)$$

On the other hand, the charge transfer energy Δ corresponds to the insulating energy gap due to the fluctuation

$$f_i^n \leftrightarrow f_i^{n+1}\underline{L}\,.$$

In Fig. 5, we show $U_{\rm eff}$ and Δ for $ThO_2 \sim BkO_2$. For ThO_2 and UO_2, $U_{\rm eff}$ is smaller than Δ, so that the minimum gap is given by the correlation gap, and such a system is denoted by the Mott-Hubbard-type insulator.[13] For PuO_2, AmO_2, CmO_2 and BkO_2, on the other hand, Δ is smaller than $U_{\rm eff}$, so that the minimum gap is the charge transfer gap, and these materials are the charge-transfer-type insulators.[13] Therefore, we find a crossover between Mott-Hubbard-type and charge-transfer-type systems around NpO_2.

§ 4. 3*d*-XPS for rare-earth sesqui-oxides

In this section we briefly review the analysis of the rare-earth $3d$-XPS for the R_2O_3 series by Ikeda et al.,[4),5)] and compare the result with that of the actinide $4f$-XPS for AnO_2 described in § 3. The model is the same as that given in § 2.1 except that the exchange interaction J is disregarded for simplicity.

The calculated results for $3d$-XPS of R_2O_3 for R=La, Ce, Pr, Nd, Sm, Eu, Gd and Yb are shown in Figs. 6(a)~(h) with the solid curve and compared with the experimental $3d_{5/2}$-XPS[14)~17)] plotted with the dashed curve ($3d_{3/2}$-XPS is not shown here). In Fig. 6 the zero of the binding energy scale E_B is taken to be the position of the higher intensity peak, and the maximum intensities of the theoretical and experimental spectra are normalized so as to be the same. For La_2O_3, Ce_2O_3, Pr_2O_3 and Nd_2O_3, two XPS peaks are observed. The intensity ratio of the lower binding energy peak to the higher one is about 1.2 for La_2O_3, but it decreases monotonically when we go from La_2O_3 to Nd_2O_3, and for Sm_2O_3 the lower binding energy peak disappears. For Eu_2O_3, however, a lower binding energy peak occurs again. From Gd_2O_3 to Er_2O_3, only a single peak is observed,[17] although the results for $Tb_2O_3 \sim Er_2O_3$ are not shown in Fig. 6. For Yb_2O_3 a weak satellite is found on the lower energy side of the main peak.

The parameter values used in this analysis is listed in Table II. Comparing between Tables I and II, we find that V of R_2O_3 is much smaller than that of AnO_2, and that U and U_{fc} of R_2O_3 are much larger than those of AnO_2. These results reflect that the spatial extension of the $4f$ wavefunction of R_2O_3 is smaller than the $5f$ wavefunction of AnO_2. Therefore, the effect of the hybridization in R_2O_3 is, in general, much smaller than that in AnO_2, and the states $|g\rangle$ and $|f\rangle$ are considerably well described within the basis space of $|f^n\rangle$ and $|f^{n+1}\underline{L}\rangle$, while more basis states are necessary for AnO_2. The value Δ decreases from La_2O_3 to Eu_2O_3, jumps to a larger value at Gd_2O_3, and decreases again from Gd_2O_3 to Yb_2O_3. Although the effect of J is not explicitly taken into account, the jump of Δ at Gd_2O_3 reflects implicitly this effect, similarly to the jump of Δ at BkO_2 as shown in § 3.

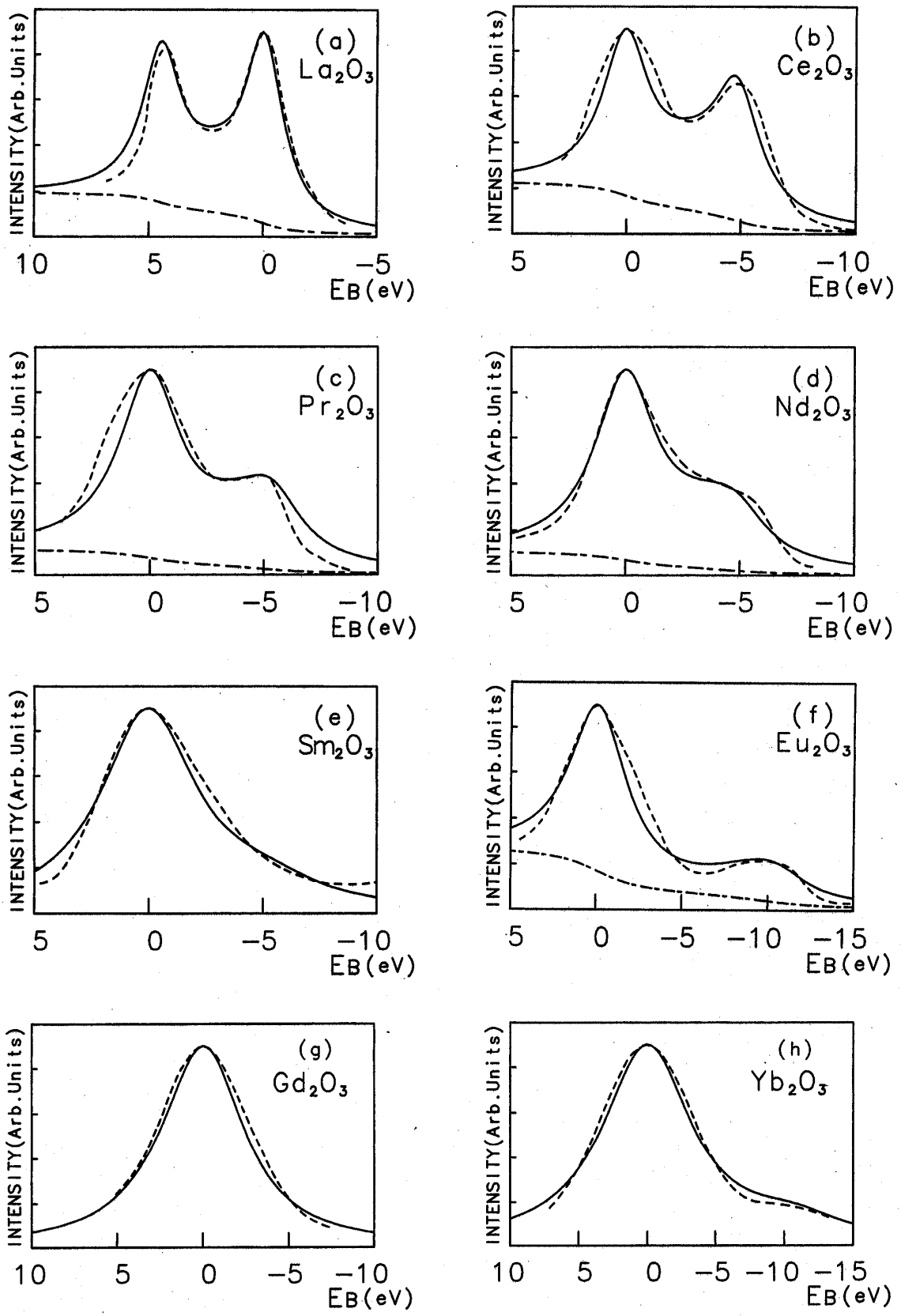

Fig. 6. Theoretical (solid curve) and experimental (dashed curve) results of $3d$-XPS for (a) La_2O_3, (b) Ce_2O_3, (c) Pr_2O_3, (d) Nd_2O_3, (e) Sm_2O_3, (f) Eu_2O_3, (g) Gd_2O_3 and (h) Yb_2O_3. The background is shown with the chain curve. The experimental data for (a), (b) (c) and (d) are taken from Ref. 14), and those for (e), (f), (g) and (h) are from Refs. 15), 16), 17) and 17), respectively.

Table II. The parameter values for R_2O_3 (R=La~Gd, Yb) estimated from the present analysis (in units of eV except for n and n_f).

	n	Δ	Δ_f	V	U	U_{fc}	W	n_f
La	0	12.5	−0.2	0.57	10.5	12.7	2.5	0.03
Ce	1	11.0	−0.9	0.6	9.1	12.0	3.0	1.04
Pr	2	10.5	−2.4	0.56	9.5	12.9	3.0	2.03
Nd	3	9.5	−2.5	0.48	10.5	12.0	3.0	3.03
Sm	5	6.5	−4.5	0.3	10.0	11.0	3.0	5.02
Eu	6	2.3	−8.7	0.3	10.0	11.0	3.0	6.14
Gd	7	13.0	2.0	0.3	10.0	11.0	3.0	7.00
Yb	13	1.7	−9.8	0.3	10.0	11.5	3.0	13.05

The splitting of $3d$-XPS in La_2O_3~Nd_2O_3 and that in Eu_2O_3 and Yb_2O_3 are explained by the two different mechanisms. For La_2O_3~Nd_2O_3, Δ is much larger than $V_{\rm eff}$ $(=\sqrt{14-n}\,V)$, so that the ground state is in the almost pure $|4f^n\rangle$ state. On the other hand, $|\Delta_f|(=|\Delta-U_{fc}|)$ is comparable with $V_{\rm eff}$, so that $|4f^n\rangle$ and $|4f^{n+1}\underline{L}\rangle$ states are mixed in the final state of $3d$-XPS. The two peaks of $3d$-XPS correspond to the bonding and antibonding states between $|4f^n\rangle$ and $|4f^{n+1}\underline{L}\rangle$ states. Thus, the splitting of $3d$-XPS is caused by the effect of the final state mixing. In the case of La_2O_3, the value of Δ_f is almost vanishing, so that the $|4f^n\rangle$ and $|4f^{n+1}\underline{L}\rangle$ states are mixed very strongly in the final state, resulting in the XPS peaks with almost the same intensities. This is in contrast to the case of ThO_2, where $\Delta_f(=4.0\,\text{eV})$ is not very small because of the small value of U_{fc}, so that the lower energy XPS peak corresponding mainly to the $|4f^n\rangle$ state is much stronger than the higher energy peak. When we go from La_2O_3 to Nd_2O_3, the final state mixing becomes weaker, because $|\Delta_f|$ increases and $V_{\rm eff}$ decreases. As a result, the relative intensity of the lower binding energy peak becomes smaller, since the final state of this peak has the increasingly larger weight of $|4f^{n+1}\underline{L}\rangle$ state which is orthogonal with the ground state. For Sm_2O_3, the intensity of the lower energy peak vanishes.

For Eu_2O_3 and Yb_2O_3, $|\Delta_f|$ is much larger than $V_{\rm eff}$, but Δ is not so large as $|\Delta_f|$ and the effect of $V_{\rm eff}$ is not negligible in the ground state. Therefore, the ground state is a mixed state between $|4f^n\rangle$ and $|4f^{n+1}\underline{L}\rangle$ states, although the mixing is not very large. The ground state has a finite overlap integrals with both of the almost pure $|4f^n\rangle$ and $|4f^{n+1}\underline{L}\rangle$ final states, resulting in the splitting of $3d$-XPS. Thus, the splitting is caused by the effect of the initial state mixing.

In contrast to the situation in R_2O_3, the splitting of $4f$-XPS in most of AnO_2 cannot be ascribed to the initial or final state mixing only; both the initial and final state mixings are important as shown in § 3.

In th rest of this section, it should be mentioned that the existence of the satellite in $3d$-XPS of Eu_2O_3 and Yb_2O_3 has not been well established. Schneider et al.[16] observed the satellite in Eu_2O_3, which we have shown in Fig. 6(f) but Osterwalder et al.[18] did not observe such a satellite. We cannot exclude the possibility that the satellite is not of instrinsic bulk origin but due to some extrinsic effect, for instance,

due to divalent rare-earth atoms at the surface. From a theoretical viewpoint, the existence of the satellite is also somewhat a subtle problem, because the intensity of the satellite depends strongly on the parameters Δ and $V_{\rm eff}$ as shown by Ikeda et al.[4] What we can say definitely is that if the satellite in Eu_2O_3 and Yb_2O_3 is intrinsic, then our mechanism (due to the initial state mixing) is the most probable one. It is highly desirable to check experimentally whether the satellite is intrinsic or not.

§ 5. Concluding remarks

In the present paper, we have carried out a systematic analysis of $4f$-XPS for AnO_2 (An=Th~Bk) with the impurity Anderson model. The effect of the exchange interaction J is shown to be important in explaining the observed $4f$-XPS especially for PuO_2, AmO_2 and CmO_2. Although our analysis is almost satisfactory, there are still some discrepancies between experimental and theoretical results. For instance, the experimental intensity ratio between $4f_{7/2}$ and $4f_{5/2}$ spectral components deviates from the statistical ratio 4:3 for some AnO_2, especially for AmO_2. It is left to future investigation to improve the analysis by explicitly taking account of the spin-orbit interaction and multipole Coulomb and exchange interactions.

The result for $4f$-XPS of AnO_2 was compared with the previous result for $3d$-XPS of R_2O_3 (R=La~Yb). Both for AnO_2 and R_2O_3, the charge transfer energy Δ decreases with increasing atomic number, and jumps for half-filled elements (Gd and Bk). The hybridization strength V for AnO_2 is larger than that for R_2O_3, and Coulomb interactions U and U_{fc} for AnO_2 are smaller than those for R_2O_3. In the previous analysis[4),5)] of $3d$-XPS of R_2O_3, the effect of J was disregarded. For $3d$-XPS of R_2O_3, however, the conspicuous splitting of XPS spectra is observed for La_2O_3, Ce_2O_3 and Pr_2O_3, where the $4f$ electron number is small, so that the effect of J is not very important. As a matter of fact, full multiplet coupling calculations of $3d$-XPS for La_2O_3, Ce_2O_3 and Pr_2O_3 have recently been carried out,[19),20)] and it was shown that the analysis without multiplet coupling (so that without J) works sufficiently well in order to estimate the parameters Δ, V, U, etc. for these materials.

Acknowledgements

The authors would like to thank Dr. K. Okada, Mr. T. Ikeda and Mr. H. Ogasawara for discussions and collaborations. This work is partially supported by the Grant-in-Aid for Scientific Research from the Ministry of Education, Science and Culture.

Appendix

Matrix elements of the Hamiltonian H_0 in our basis space are given here. The diagonal matrix elements are as follows:

$$\langle f^n|H_0|f^n\rangle = n\varepsilon_f + \frac{1}{2}n(n-1)(U-J) + 2N_f\sum_k \varepsilon_v(k) \equiv E_0\,,$$

$$\langle f^{n+1}\uparrow \underline{L}(k)|H_0|f^{n+1}\uparrow \underline{L}(k)\rangle = E_0+\varepsilon_f-\varepsilon_v(k)+nU-nJ\,,$$

$$\langle f^{n+1}\downarrow \underline{L}(k)|H_0|f^{n+1}\downarrow \underline{L}(k)\rangle = E_0+\varepsilon_f-\varepsilon_v(k)+nU\,,$$

$$\langle f^{n+2}\uparrow\uparrow \underline{L}(k,l)|H_0|f^{n+2}\uparrow\uparrow \underline{L}(k,l)\rangle = E_0+2\varepsilon_f-\varepsilon_v(k)-\varepsilon_v(l)+(2n+1)U-(2n+1)J\,,$$

$$\langle f^{n+2}\uparrow\downarrow \underline{L}(k,l)|H_0|f^{n+2}\uparrow\downarrow \underline{L}(k,l)\rangle = E_0+2\varepsilon_f-\varepsilon_v(k)-\varepsilon_v(l)+(2n+1)U-nJ\,,$$

$$\langle f^{n+2}\downarrow\downarrow \underline{L}(k,l)|H_0|f^{n+2}\downarrow\downarrow \underline{L}(k,l)\rangle = E_0+2\varepsilon_f-\varepsilon_v(k)-\varepsilon_v(l)+(2n+1)U-J\,,$$

$$\langle f^{n+3}\uparrow\uparrow\uparrow \underline{L}(k,l,m)|H_0|f^{n+3}\uparrow\uparrow\uparrow \underline{L}(k,l,m)\rangle = E_0+3\varepsilon_f-\varepsilon_v(k)-\varepsilon_v(l)-\varepsilon_v(m)+3(n+1)U-3(n+1)J\,,$$

$$\langle f^{n+3}\uparrow\uparrow\downarrow \underline{L}(k,l,m)|H_0|f^{n+3}\uparrow\uparrow\downarrow \underline{L}(k,l,m)\rangle = E_0+3\varepsilon_f-\varepsilon_v(k)-\varepsilon_v(l)-\varepsilon_v(m)+3(n+1)U-(2n+1)J\,,$$

$$\langle f^{n+3}\uparrow\downarrow\downarrow \underline{L}(k,l,m)|H_0|f^{n+3}\uparrow\downarrow\downarrow \underline{L}(k,l,m)\rangle = E_0+3\varepsilon_f-\varepsilon_v(k)-\varepsilon_v(l)-\varepsilon_v(m)+3(n+1)U-(n+1)J\,,$$

$$\langle f^{n+3}\downarrow\downarrow\downarrow \underline{L}(k,l,m)|H_0|f^{n+3}\downarrow\downarrow\downarrow \underline{L}(k,l,m)\rangle = E_0+3\varepsilon_f-\varepsilon_v(k)-\varepsilon_v(l)-\varepsilon_v(m)+3(n+1)U-3J\,.$$

Non-zero off-diagonal matrix elements are written as

$$\langle f^{n}|H_0|f^{n+1}\uparrow \underline{L}(k)\rangle = V\sqrt{\frac{N_f-n}{N}}\,,$$

$$\langle f^{n}|H_0|f^{n+1}\downarrow \underline{L}(k)\rangle = V\sqrt{\frac{N_f}{N}}\,,$$

$$\langle f^{n+1}\uparrow \underline{L}(k)|H_0|f^{n+2}\uparrow\uparrow \underline{L}^2(l,m)\rangle = V\sqrt{\frac{N_f-n-1}{N}}\delta_2(l,m)(\delta_{kl}+\delta_{km})\,,$$

$$\langle f^{n+1}\downarrow \underline{L}(k)|H_0|f^{n+2}\downarrow\downarrow \underline{L}^2(l,m)\rangle = V\sqrt{\frac{N_f-1}{N}}\delta_2(l,m)(\delta_{kl}+\delta_{km})\,,$$

$$\langle f^{n+1}\uparrow \underline{L}(k)|H_0|f^{n+2}\uparrow\downarrow \underline{L}^2(l,m)\rangle = V\sqrt{\frac{N_f}{N}}\delta_{kl}\,,$$

$$\langle f^{n+1}\uparrow \underline{L}(k)|H_0|f^{n+2}\uparrow\downarrow \underline{L}^2(l,m)\rangle = V\sqrt{\frac{N_f-n}{N}}\delta_{km}\,,$$

$$\langle f^{n+2}\uparrow\uparrow \underline{L}^2(k,l)|H_0|f^{n+3}\uparrow\uparrow\uparrow \underline{L}^3(m,i,j)\rangle = V\sqrt{\frac{N_f-n-2}{N}}\delta_2(k,l)\delta_3(m,i,j)\times((L^{li}_{km}+L^{lm}_{ki})+(m,i,j \text{ cyclic}))\,,$$

$$\langle f^{n+2}\downarrow\downarrow \underline{L}^2(k,l)|H_0|f^{n+3}\downarrow\downarrow\downarrow \underline{L}^3(m,i,j)\rangle = V\sqrt{\frac{N_f-2}{N}}\delta_2(k,l)\delta_3(m,i,j) \times((L^{li}_{km}+L^{lm}_{ki})+(m,i,j \text{ cyclic}))\,,$$

$$\langle f^{n+2}\uparrow\uparrow \underline{L}^2(k,l)|H_0|f^{n+3}\uparrow\uparrow\downarrow \underline{L}^3(m,i,j)\rangle = V\sqrt{\frac{N_f}{N}}\delta_2(k,l)\delta_2(m,i)(L^{li}_{km}+L^{lm}_{ki})\,,$$

$$\langle f^{n+2}\downarrow\downarrow \underline{L}^2(k,l)|H_0|f^{n+3}\uparrow\downarrow\downarrow \underline{L}^3(m,i,j)\rangle = V\sqrt{\frac{N_f-n}{N}}\delta_2(k,l)\delta_2(i,j)(L^{lj}_{ki}+L^{li}_{kj})\,,$$

$$\langle f^{n+2}\uparrow\downarrow \underline{L}^2(k,l)|H_0|f^{n+3}\uparrow\uparrow\downarrow \underline{L}^3(m,i,j)\rangle = V\sqrt{\frac{N_f-n-1}{N}}\delta_2(m,i)(L^{lj}_{ki}+L^{lj}_{km})\,,$$

$$\langle f^{n+2}\uparrow\downarrow \underline{L}^2(k,l)|H_0|f^{n+3}\uparrow\downarrow\downarrow \underline{L}^3(m,i,j)\rangle = V\sqrt{\frac{N_f-n-1}{N}}\delta_2(i,j)(L^{li}_{km}+L^{lj}_{km})\,,$$

where

$$L^{kl}_{ij}=\delta_{ij}\delta_{kl}\,,$$

$$\delta_3(k,l,m)=\begin{cases}1 & \text{for } k\neq l\neq m\neq k\,,\\ 1/\sqrt{2} & \text{for } k=l\neq m \text{ and } (k,l,m) \text{ cyclic}\,,\\ 1/\sqrt{6} & \text{for } k=l=m\,,\end{cases}$$

and $\delta_2(k,l)$ is given by Eq. (2·12).

Matrix elements of the Hamiltonian H are obtained from those of the Hamiltonian H_0 simply by replacing ε_f with ε_f-U_{fc}.

References

1) See, for instance, *Core-Level Spectroscopy in Condensed Systems*, ed. J. Kanamori and A. Kotani (Springer-Verlag, 1988).
2) A. Kotani, T. Jo and J. C. Parlebas, Adv. Phys. **37** (1988), 37.
3) J. Zaanen, C. Westra and G. A. Sawatzky, Phys. Rev. **B33** (1986), 8060.
4) T. Ikeda, K. Okada, H. Ogasawara and A. Kotani, J. Phys. Soc. Jpn. **59** (1990), 622.
5) A. Kotani, T. Ikeda, K. Okada and H. Ogasawara, J. Electron Spectroscopy and Related Phenomena **52** (1990), 313.
6) A short report has been published: T. Yamazaki and A. Kotani, J. Phys. Soc. Jpn. **60** (1991), 49.
7) O. Gunnarsson and D. D. Sarma, J. Appl. Phys. **63** (1988), 3676.
8) Y. Baer, J. Schoenes, Solid State Commun. **33** (1980), 885.
9) B. W. Veal, D. J. Lam, H. Diamond and H. R. Hoekstra, Phys. Rev. **B15** (1977), 2929.
10) D. van der Marel, Doctor Thesis, University of Groningen (1985).
11) A. Bianconi, A. Kotani, K. Okada, R. Giorgi, A. Gargano, A. Marcelli and T. Miyahara, Phys. Rev. **B38** (1988), 3433.
12) B. Johansson, J. Phys. Chem. Solids **39** (1978), 467.
13) J. Zaanen, G. A. Sawatzky and J. W. Allen, Phys. Rev. Lett. **55** (1985), 418.
14) J. C. Fuggle, M. Campagna, Z. Zolnierek, R. Lässer and A. Platru, Phys. Rev. Lett. **45** (1980), 1597.
15) M. Aono, S. Kawai, S. Kono, M. Okusawa, T. Sagawa and Y. Takehara, Solid State Commun. **16** (1974), 13.
16) W. D. Schneider, C. Laubsschat, I. Nowik and G. Kaindl, Phys. Rev. **B24** (1981), 5422.

17) T. Takahashi, M. Fujinami, H. Arai, S. Hashiguchi and T. Ohtsubo, Autum Meeting of Phys. Soc. Jpn. (1988), 6a C3-17.
18) J. Osterwalder, A. Wisard, E. Jilek and P. Wachter, J. Magn. Magn. Mater. **47&48** (1985), 586.
19) S. Imada and T. Jo, J. Phys. Soc. Jpn. **58** (1989), 402, 2665.
20) H. Ogasawara, A. Kotani, R. Potze, G. A. Sawatzky and B. T. Thole, Phys. Rev. **B44** (1991), 5465.